This is a preprint, the final version is subject to change, of the American Mineralogist (MSA)
Cite as Authors (Year) Title. American Mineralogist, in press.
DOI: https://doi.org/10.2138/am-2020-7136CCBY

Revision 1

Elastic properties of majoritic garnet inclusions in diamonds and the seismic signature of pyroxenites in the Earth's upper mantle

Iuliia Koemets[1], Niccolò Satta[1], Hauke Marquardt[1,2], Ekaterina S. Kiseeva[2,3,*], Alexander Kurnosov[1], Thomas Stachel[4], Jeff W. Harris[5] and Leonid Dubrovinsky[1]

[1]Bayerisches Geoinstitut, University of Bayreuth, 95440 Bayreuth, Germany
[2]University of Oxford, Department of Earth Sciences, South Parks Road, Oxford, UK
[3]University College Cork, School of Biological, Earth and Environmental Sciences, Distillery Fields, North Mall, Cork, T23 N73K, Ireland
[4]Department of Earth and Atmospheric Sciences, University of Alberta, Edmonton, AB, T6G 2E3, Canada
[5]School of Geographical and Earth Sciences, University of Glasgow, Glasgow, G12 8QQ, UK
[*]Corresponding author: kate.kiseeva@ucc.ie

Abstract

Majoritic garnet has been predicted to be a major component of peridotite and eclogite in Earth's deep (>250 km) upper mantle and transition zone. The investigation of mineral inclusions in diamond confirms this prediction, but there is reported evidence of other majorite-bearing lithologies, intermediate between peridotitic and eclogitic, present in the mantle transition zone. If these lithologies are derived from olivine-free pyroxenites, then at mantle transition zone pressures majorite may form monomineralic or almost monomineralic garnetite layers. Since majoritic garnet is presumably the seismically fastest major phase in the lowermost upper mantle, the existence of such majorite layers might produce a detectable seismic signature. However, a test of this hypothesis is hampered by the absence of sound wave velocity measurements of majoritic garnets with relevant chemical compositions, since previous measurements have been mostly limited to synthetic majorite samples with relatively simple compositions. In an attempt to evaluate the seismic signature of a pyroxenitic garnet layer, we measured the sound wave velocities of three natural majoritic garnet inclusions in diamond by Brillouin spectroscopy at ambient conditions. The chosen natural garnets derive from depths between 220 km and 470 km and are plausible candidates

DOI: https://doi.org/10.2138/am-2020-7136CCBY

to have formed at the interface between peridotite and carbonated eclogite. They contain elevated amounts (12-30%) of ferric iron, possibly produced during redox reactions that form diamond from carbonate. Based on our data, we model the velocity and seismic impedance contrasts between a possible pyroxenitic garnet layer and the surrounding peridotitic mantle. For a mineral assemblage that would be stable at a depth of 350 km, the median formation depth of our samples, we found velocities in pyroxenite at ambient conditions to be higher by 2.2(6)% for shear waves and 3.6(5)% for compressional waves compared to peridotite (numbers in brackets refer to uncertainties in last given digit), and by 2.3(13)% for shear waves and 3.4 (10)% for compressional waves compared to eclogite. As a result of increased density in the pyroxenitic layer, expected seismic impedance contrasts across the interface between the monomineralic majorite layer and the adjacent rocks are about 4-5% at the majorite-eclogite-interface and 10-12% at the majorite-peridotite-boundary. Given a large enough thickness of the garnetite layer, velocity and impedance differences of this magnitude could become seismologically detectable.

Introduction

Majoritic garnet is one of the main constituents of the lowermost upper mantle and the mantle transition zone, comprising up to 35 vol% in peridotitic and up to 95 vol% in eclogitic lithologies (Wood *et al*., 2013). Despite having a wide stability field (~7-26 GPa) and being one of the most common minerals in Earth's mantle, the compositions of natural majoritic garnets are not very well-known and there are only a few findings of this mineral as inclusions in diamond. To date, there are only about 150 majoritic garnet inclusions in diamonds reported in the literature (Kiseeva *et al*., 2013) with the majority of them having either eclogitic (metabasaltic) or pyroxenitic paragenesis; observations of majoritic garnets of peridotitic paragenesis are rare and invariably relate to depleted (lithospheric mantle-like) substrates instead of pyrolite.

The compositions of majoritic garnets vary substantially. If a generic mineral formula for upper mantle garnets is described as $(Mg,Ca,Fe^{2+})_3(Al,Cr, Fe^{3+})_2(SiO_4)_3$, majoritic garnet will contain Si and Mg on the octahedral site, and in more eclogitic compositions, Na on the dodecaheral site, resulting in a more complicated solid solution $(Na,Mg,Ca,Fe^{2+})_3(Al,Cr,Fe^{3+},Si,Mg)_2(SiO_4)_3$. Monovalent Na is charge-balanced through the coupled substitution: $Na^+ + Si^{4+} = Al^{3+} + Mg^{2+}$. In Na-poor compositions, a more divalent cation-rich (Mg, Ca, Fe^{2+}) majoritic garnet is formed, following the substitution: $Si^{4+} + M^{2+} = 2Al^{3+}$, where M^{2+} is usually Mg.

With increasing depth, the stabilisation of more ferric iron-rich andradite ($Ca_3Fe_2(SiO_4)_3$) and/or skiagite ($Fe_3Fe_2(SiO_4)_3$) components occur at the expense of Al-rich pyrope and almandine (Woodland and O'Neill, 1993; Kiseeva *et al.*, 2018). In their recent study on majoritic inclusions in diamond, Kiseeva *et al.* (2018) showed that the amount of ferric iron in majorites increases from molar $Fe^{3+}/(Fe^{3+}+ Fe^{2+})$ of 0.08 at approximately 240 km depth to 0.30 at approximately 500 km depth.

The deepest majorites, derived from the transition zone, are of pyroxenitic origin (Kiseeva *et al.*, 2013; 2016). There are a number of mechanisms proposed which result in the formation of pyroxenitic lithologies, one of them being through the interaction of mantle peridotite with eclogite, or eclogite-derived melts, the latter introduced into the mantle by subduction (Yaxley and Green, 1998; Thomson *et al*., 2016). In their study on peridotite-eclogite interaction, Kiseeva *et al*. (2016) showed that pyroxenitic garnet will crystallise as a monomineralic layer at the reaction boundary between peridotite and a carbonated eclogite. Thomson *et al.* (2016) studied the products of peridotite interaction with carbonatitic melt produced by melting of carbonated subducted crust and showed that the compositions of the resulting majoritic garnets were also broadly pyroxenitic. These authors further suggested that due to highly reducing conditions in the lowermost upper mantle and the mantle transition zone, the carbonatitic melts will also produce diamond upon reaction with ambient pyrolitic mantle (Rohrbach and Schmidt, 2011). Thus, if such scenarios are common and subducting slabs indeed expel pulses of low-degree melts upon their descent into the deep mantle (e.g. Thomson *et al.*, 2016), monomineralic lenses of garnetite and/or olivine-free pyroxenite are expected to form along the reaction fronts. At pressures exceeding the stability of pyroxenes, majoritic garnet of broadly pyroxenitic composition may be the only mineral present in the reaction zones, possibly accompanied by small amounts of stishovite or olivine/wadsleyite, depending on the bulk rock composition (Fig. 1). Although peridotite-eclogite interaction in the presence of carbonatitic melts is a plausible scenario of pyroxenite formation in the upper mantle and the mantle transition zone, other mechanisms should not be disregarded. Hirschmann and Stolper (1996) list a number of processes leading to pyroxenite formation in the asthenosphere, among which subduction of oceanic crust and veined oceanic lithosphere, delamination of continental crust and subcontinental mantle, exhumation of the mantle wedge material and metamorphic segregation. Furthermore, the authors suggest that pyroxenites may constitute 2-5% of the upper mantle, being present in the form of layers and lenses within mantle peridotites. If this material is transported to larger depths, outside of the stability field of pyroxene, the pyroxenitic layers of various compositions will be transformed into layers of pure garnetite (in compositions closer to eclogite) and garnet and olivine (in compositions closer to peridotite). Using the database of majoritic inclusions in diamonds, Kiseeva et al (2016) recalculated the composition of parental lithology for ~80 majoritic inclusions, concluding that they span a wide range of intermediate compositions between typical eclogite and peridotite, from ~ 90% eclogite to 70% peridotite, and that most of them could have derived from monomineralic garnetite, without having been in equilibrium with a clinopyroxene. This confirms the potential for the presence of monomineralic garnetite layers in the lowermost upper mantle and transition zone. However, neither the shapes and sizes of the garnetite bodies nor their abundance in the mantle are known.

One way to enable the hypothesis of the presence of garnetite layers of pyroxenitic composition in the mantle transition zone to be tested is through an investigation of the expected seismic signature of such majoritic garnets. Because the pyroxene-garnet transition is gradual and occurs over a large pressure interval, there is no seismic discontinuity associated with the formation of majoritic garnet. However, due to its large modal abundance, majoritic garnet can have a profound effect on sound velocities and cause high velocity gradients in the transition zone (Irifune, 1987).

Multiple studies on elastic properties of upper mantle garnet end-members have shown that compressional wave (Vp) and shear-wave velocities (Vs) are strongly composition-dependent and substantially differ between the garnet end-members (Vs = 4.6-5.5 km/s and Vp = 8.3-9.3 km/s) (Wang and Ji, 2001). It is, however, not well known how variations in composition affect sound velocities of majoritic garnet (Irifune et al., 2008). There are only a few studies of elastic properties of majoritic garnets, with most of them being conducted on synthetic samples, investigating either end-members or relatively simple solid-solutions (e.g. Sinogeikin and Bass, 2002; Irifune *et al*., 2008; Murakami *et al*., 2008; Pamato *et al*., 2016; Vasiukov *et al*., 2018; Liu et al., 2019; Sanchez-Valle et al., 2019). The scarcity of sound wave velocity data on natural majorites is due to the rarity of samples and very small crystal sizes (<200 microns).

To date, elasticity measurements of natural majorites were only obtained on Mg-rich polycrystalline samples from the Catherwood meteorite with no data being available for natural single-crystal majorites (Kavner *et al*., 2000; Sinogeikin and Bass, 2002).

Given the role of majoritic garnet as a rock-forming mineral in the Earth's mantle at depths of ~300-750 km, and as a key host for a wide array of both compatible and incompatible elements, the purpose of this study is to determine the elastic properties of natural single-crystal majoritic garnets and to test whether garnetite layers, formed as a result of the pyroxenite – garnetite transformation at the pressures of the mantle transition zone could be seismically detectable.

Materials and Methods

Samples. For this study, we selected three natural single-crystal majoritic garnet inclusions in diamonds (37B, 39A and 55A) from the Jagersfontein kimberlite in South Africa (Supplementary Table 1 and Table 1). The inclusions were about 100-120 µm in size and optically transparent (Fig 2 and optical images in Kiseeva et al. (2018)). For previous studies, the inclusions were separated from the host diamond, mounted in epoxy disks with 0.7 mm thickness supported by brass rings and then polished on one side. For Brillouin scattering measurements, the crystals were released from the initial epoxy and polished on both sides to a thickness of 50-30 µm.

The crystals were previously analysed by electron microprobe for major element compositions (Tappert et al., 2005), by X-ray diffraction (XRD) for structure, and by synchrotron Mössbauer source (SMS) spectroscopy (beamline ID18 at the European Synchrotron Radiation Facility, Grenoble) for ferric-ferrous ratios (Kiseeva et al., 2018). The XRD analysis conducted at beamline P02 at PETRA III, Hamburg confirmed the majorites as monophase single crystals (Kiseeva et al., 2018). Major element compositions, ferric-ferrous ratios and garnet components of the studied majorites are summarised in Table 1 and Supplementary Table 1.

The majoritic garnets are of pyroxenitic composition and contain relatively high concentrations of CaO (5.7-7.3 wt%), but low Cr_2O_3 (0.13-0.36) with up to 0.1-0.4 wt% Na_2O and intermediate Mg# (0.70-0.81). Ferric iron content is 12-30% of total iron, as opposed to 5-10% in typical upper mantle (Canil and O'Neill, 1996; Kiseeva et al., 2018). More details about these inclusions and their host diamonds can be found in Tappert et al. (2005) and Kiseeva et al. (2018). The pressure of the last equilibration of these majorites was determined using the geobarometer of Beyer and Frost (2017) (Supplementary Table 1). This geobarometer is based on experimentally synthesised garnet-clinopyroxene pairs. However, given that the studied inclusions are single grains (no coexisting clinopyroxene inclusions), all clinopyroxene in the source regions may have already completely dissolved in garnet, rendering the calculated pressures minimum pressures (Beyer and Frost, 2017).

The origins of these inclusions were previously addressed by studies of their oxygen isotope composition (Ickert et al., 2015) and the carbon isotope composition of their enclosing diamond (Tappert et al. 2005). These isotopic signatures suggest a subduction origin, which indicates that the studied majoritic garnets could be plausible candidates to have formed through the pyrolite-metabasalt interaction mechanism. Formation through the reaction of slab derived carbonatitic melts and ambient mantle is supported by elevated amounts of ferric iron in majorite, possibly produced as oxidation of Fe^{2+} into Fe^{3+} upon reduction of carbon from carbonate into diamond (Kiseeva *et al*., 2018).

Brillouin scattering. Elastic wave velocities were measured in forward symmetric scattering geometry (Whitfield et al., 1976; Speziale et al., 2014) using the Brillouin system at BGI Bayreuth. The wavelength of the (Nd: YVO4) laser light was 532 nm. The power of the incident beam measured before the sample was 30-60 mW. A multipath tandem Fabry-Perot interferometer (Lindsay et al., 1981) was used to solve Brillouin frequency shifts, and a single photon counting module was employed for signal detection, respectively.

Although uncertainties on measurements derived from signal-to-noise ratio are in general less than 1% (Table 2), due to the small size of the crystals and high risk of sample loss during sample preparation, the polished surfaces were relatively small in comparison to the thickness of the crystals. This causes occasional deviations from the perfect platelet scattering geometry that is required for Brillouin spectroscopy measurements (Whitfield et al., 1976; Speziale et al., 2014), and may explain the scatter seen in the obtained sound velocities (Table 2, Supplementary Figure 1).

Considering that the scatter appears random, and garnets generally show weak elastic anisotropy (Murakami et al., 2008), we assume that the variation of measured velocities with direction is caused by the deviation from ideal platelet geometry rather than an intrinsic elastic anisotropy (which should follow a more systematic trend).

In order to compromise between data quality and sample preservation, we used the least possible and safe polishing and compensated it with multiple (13-19) measurements along 360 degrees range of directions. Therefore, Brillouin measurements were performed in different crystallographic directions by rotating the sample within the scattering plane. Measurements were taken with a step size of about 20° over a large range of angles, covering almost the full 360° angular range.

The aggregate velocities and elastic moduli were obtained by averaging acoustic velocities over a number of crystallographic directions (e.g. Sinogeikin and Bass, 2000) and uncertainty was estimated as standard error (Table 2, Supplementary Figure 1). The resulting uncertainty values deviate from the average more than it is suggested from estimations based on signal-to-noise ratio. That is why the standard deviation from all measurements was used as an upper limit of uncertainty estimation. In the case of samples 37b and 39a, it did not exceed 1%. For the sample 55a, the measured sound velocities have a standard deviation of ~2%. We provide standard errors as a measure of uncertainty on figures and tables in the main text.

Results and Discussion

Ferric iron in natural majorites and its effect on sound velocities

It has been observed that ferric iron in majoritic garnets increases with pressure (Kiseeva *et al*., 2018). XRD diffraction patterns of the studied majorites provide estimates of the site occupancy of different elements. Given their complex chemical composition and relatively large amounts (up to 3 wt%) of minor and trace elements (Na_2O, MnO, Cr_2O_3, TiO_2, rare earth elements), it is impossible to precisely evaluate the occupancy of X and Y sites. Ferric iron on the Y-site can be present as one of three components: andradite ($Ca_3Fe_2(SiO_4)_3$), khoharite ($Mg_3Fe_2(SiO_4)_3$), or skiagite ($Fe_3Fe_2(SiO_4)_3$) among which only andradite is common in nature and its elastic properties are very well-studied. As the choice of end-members for recalculation of garnet into individual components does not affect sound velocities (Vasiukov *et al*., 2018), for simplicity, we assume that all ferric iron is present in the andradite component. The andradite component in the studied garnets is relatively small and varies between 4.6 and 8.3 mol% (Table 1).

Figure 3 shows the relationship of sound velocities, measured at ambient conditions, with the pressure of last equilibration. There appear to be no correlations among velocity, pressure of formation, and ferric iron content. This is consistent with our estimate that ferric iron ratios of 30% in our deepest samples will translate to ~8% andradite component only (Table 1, Supplementary Table 1). Due to the small differences in sound velocities with almandine and pyrope, such a small andradite component will not be detectable by seismic measurements.

Sound velocities of end-members and solid solutions

Over the last decades, the elastic properties of upper mantle garnet end-members have been relatively well-investigated at physical conditions relevant for the Earth's interior, and are generally consistent with each other (Wang and Ji, 2001). The complexity of natural garnet

This is a preprint, the final version is subject to change, of the American Mineralogist (MSA)
Cite as Authors (Year) Title. American Mineralogist, in press.
DOI: https://doi.org/10.2138/am-2020-7136CCBY

chemical composition necessitates the ability to transfer the elastic properties of individual end-members to solid solutions (e.g. Chantel et al., 2016, Pamato et al., 2016). At ambient conditions, it has been shown that the elastic properties of the members of the pyralspite garnet series (pyrope-almandine-spessartine) are linearly dependent on the properties of the end-members (Erba et al., 2014).

In this study, we compared the measured sound velocities for the natural majoritic garnets with the sound velocities calculated from individual end-members. We calculated physical parameters (A), i.e. density and elastic moduli of our majoritic garnets as $A = \sum_{i=1}^{N} m_i A_i$. This approach involves the use of the molar end-member fraction (m_i) and physical parameters of the i-th constituent (A_i), which are listed in Tables 1 and 3 respectively. We then use the calculated physical parameters to determine $V_P = \sqrt{\frac{K+4G/3}{\rho}}$ and $V_S = \sqrt{\frac{G}{\rho}}$ of our majoritic garnets. The measured and calculated sound velocities are in good agreement (Supplementary Table 2). This suggests that, at least at ambient conditions, the linear relationship between solid solutions and end-members observed for the upper mantle garnets can be extrapolated to majoritic garnets from the mantle transition zone.

Some experimental data exist on the elasticity of majoritic garnets at high-pressure and high-temperature (Pamato et al., 2016, Irifune et al., 2008), but the available data do not allow for a comprehensive evaluation of the effects of chemical variabilities on elasticity. The here-presented calculations are, therefore, performed for ambient conditions. The results can serve to guide future work but might need revision once more comprehensive data on the elasticity of majoritic garnets at conditions of the upper mantle become available. We note that few studies suggest more complicated mixing behaviours at high-pressure/-temperature. For example, the elasticity of pyralspite garnets shows a more complicated behaviour which cannot be approximated with a linear function (Du et al., 2015).

Implications for the seismic detection of pyroxenite in the deep upper mantle

As confirmed by our measurements on natural majoritic garnets from the deep upper mantle and transition zone, majorite shows the highest elastic wave velocities among all major upper mantle phases. This opens the possibility that pyroxenitic, or monomineralic garnet layers lead to a detectable seismic signature if they occur on length scales comparable to or larger than the seismic wavelength. Here, we use our results derived from natural deep mantle majorities to evaluate the possible seismic signal of majorite-rich regions. In particular, we modelled the seismic contrasts for a mineral assemblage expected at eclogite-pyroxenite and peridotite-pyroxenite interfaces at 350 km.

For the purpose of our model, we considered a scenario with eclogitic rocks being in contact with the average peridotitic mantle (Fig 4a). At the formation conditions of our garnet JF 39a (~13 GPa, 350 km depth), standard peridotitic mantle consists of 58 vol% of olivine, 12 vol% of pyroxene and 30 vol% of garnet (Frost, 2008). At the same depth, subducted eclogitic rocks are expected to have a volumetric abundance of majoritic garnets of 65% while the remaining fraction is occupied by pyroxenes and a negligible fraction of stishovite (Irifune et al., 1986). The elastic moduli K and G of these polymineralic isotropic aggregates (rocks) can be evaluated by averaging Voigt (M_V) and Reuss (M_R) bounds, which are formulated as $M_V = \sum_{i=1}^{N} M_i f_i$ and $1/M_R = \sum_{i=1}^{N} f_i/M_i$ where N is the number of different minerals in the aggregate, f_i and M_i are the volume fractions and elastic moduli of the i-th constituent (Avseth *et al.*, 2010).

Isotropic velocities of the minerals considered in our modeling are listed in Supplementary Table 2 while assumed volume fractions are reported in Supplementary Table 3. Since the here-reported measurements were performed at room conditions only, we do not have any constraints on the pressure- and temperature-dependency of the elastic properties of our samples. Therefore, we restrict our calculations to ambient conditions. Our modelling, however, accounts for variations of stable mineral assemblages with depth. The chemical composition and, as a consequence, the elastic properties, assumed for the modeled garnets reflect their geological context. Peridotitic garnets have a higher Mg# (molar Mg/(Mg+Fe), usually > 0.8, and contain relatively small amounts of Ca (up to 4-5 wt% CaO) and very high amounts of Cr (up to 20-25 wt% Cr_2O_3) when compared to eclogitic garnets that contain < 1 wt% Cr_2O_3 and up to 20 wt% CaO (Sobolev et al., 1973). Calcium, chromium and Mg# are the main discriminators between the two types of garnets, however, in addition to these, garnet compositions also differ in the concentrations of Ti, with eclogitic garnets containing up to a few percent TiO_2.

Pyroxenitic garnet is intermediate in its composition between peridotitic and eclogitic garnets, and usually exhibits intermediate CaO concentrations, low Cr-concentrations (similar but slightly higher than eclogitic garnet), but lower Ti and high Mg#, more characteristic of peridotitic garnets (Kiseeva et al., 2013; Kiseeva et al., 2016).

As a result, the pyrope, grossular, almandine and Cr-bearing knorringite/uvarovite components significantly differ for the three types of garnet. Peridotitic garnets contain a significantly larger proportion of pyrope ($Mg_3Al_2(SiO_4)_3$) and uvarovite ($Ca_3Cr_2(SiO_4)_3$) components and are poorer than eclogitic garnets in grossular ($Ca_3Al_2(SiO_4)_3$) and almandine ($Fe_3Al_2(SiO_4)_3$) components. Pyroxenitic garnets are high in pyrope and low in uvarovite.

Our results only serve as an indication of whether pyroxenite could be detectable by seismology. Resulting physical properties of the modeled mantle rocks are listed in Table 4.

As expected, we found that both P- and S-waves propagate faster in pyroxenite than in both bulk rock peridotite and eclogite at ambient conditions. Compared to peridotite, V_P and V_S in our pyroxenitic garnets are expected to be faster by 3.6(5)% and 2.2(6)%, respectively. This is because 66 vol% of a peridotite consist of olivine and clinopyroxene at 350 km depth. In these two minerals, seismic waves propagate at lower velocities than in peridotitic garnet, which constitutes the remaining volume of the bulk rock. Given a large enough thickness of the possible pyroxenitic garnetite layer, velocity differences to ambient peridotitic mantle are expected to be seismologically detectable (Wit *et al.,* 2012). When olivine transforms to wadsleyite at approximately 410 km depths, the situation changes in that pyrolite will become seismically faster by about the 2.1(8)% in V_P and 3.6(8)% in V_S than pyroxenite. Similarly, the velocity contrast between eclogite/metabasalt and pyroxenite ranges from 2.3(13)% in S-wave velocities to 3.4 (1)% in P-wave velocities. Unlike peridotitic garnet, eclogitic garnet has similar V_P and V_S as pyroxenitic garnet because of its high Fe content (28 mol.% almandine), which lowers propagation velocities of both P- and S-waves. Therefore, the velocity contrast is only due to the presence of seismically slow Ca-clinopyroxene in the eclogitic rock. The seismic reflection coefficient, however, does not depend on the velocity contrasts alone, but is rather sensitive to the impedance contrast across an interface. Pyroxenite is denser than eclogite, but also has higher bulk and shear moduli, which make it seismically faster. The impedance contrast across a possible pyroxenite-eclogite interface amounts to almost 5% for V_P and 4% for Vs, which might be strong enough for detection by seismology. The impedance contrast across a pyroxenite-peridotite interface for the mineral assemblage expected at 350 km depth is much higher and calculated to be about 12% (V_P) and 10% (Vs). The impedance contrast between pyroxenite and eclogite is expected to be strongly depth-dependent since it is sensitive to the pyroxene/garnet ratio in eclogite. Based on our modelling, a monomineralic majoritic garnet layer of sufficient size will be seismically faster, about 3% for *Vp* and 2% for *Vs,* than both peridotite and eclogite above the transition zone, with the exact values being a function of depth. In the transition zone, the situation becomes more complicated with pyrolite becoming seismically faster than majorite-garnetite, due to the olivine-wadsleyite transition (Fig. 4). Throughout the transition zone sound velocities are increasing, with a sharp rise being observed at the transition zone lower mantle boundary. The composition of the rocks in that region remains debated (e.g. Irifune, 2008), with a number of recent studies suggesting an enrichment in basaltic lithologies throughout the mantle transition zone (Ballmer et al., 2015) and at the transition zone lower mantle boundary (Greaux et al., 2019). These findings are in good agreement with the possible presence of pyroxenites in the deeper regions of the Earth.

Although our measurements and modelling were performed at ambient conditions, these first results indicate that pyroxenite layers, predicted to exist at the interface of subducting slabs and ambient convecting mantle, could be detected seismologically at depth shallower than 410 km. Future experiments and modelling at elevated pressure and temperature conditions are, however, required to put tighter quantitative constraints on the seismic signature of pyroxenite in the deep mantle.

Acknowledgments

We thank Johannes Buchen for providing wadsleyite elasticity data. We also thank Denis Vasiukov for comments and discussion. Many thanks to two anonymous reviewers for their valuable comments that significantly improved this manuscript and a special thank you to Fabrizio Nestola for editorial handling. This research was supported through the project "GeoMaX" funded under the Emmy-Noether Program of the German Science Foundation DFG (MA4534/3-1). HM acknowledges support from the Bavarian Academy of Sciences. ESK was supported by NERC grant NE/L010828/1. NS was supported by the IRTG "Deep Earth Volatile Cycles" grant (GRK 2156/1).

Bibliography

Arimoto, T., Greaux, S., Irifune, T., Zhou, C.Y., Higo, Y., 2015. Sound velocities of $Fe_3Al_2Si_3O_{12}$ almandine up to 19 GPa and 1700 K. Physics of the Earth and Planetary Interiors 246, 1-8.

Avseth, P., Mukerji, T., Mavko, G., Dvorkin, J., 2010. Rock-physics diagnostics of depositional texture, diagenetic alterations, and reservoir heterogeneity in high-porosity siliciclastic sediments and rocks - A review of selected models and suggested work flows. Geophysics 75, A31-A47.

Ballmer, M. D., N. C. Schmerr, T. Nakagawa, and J. Ritsema. Compositional mantle layering revealed by slab stagnation at similar to 1000 km depth. Science Advances 1, 11.

Beyer, C., Frost, D.J., 2017. The depth of sub-lithospheric diamond formation and the redistribution of carbon in the deep mantle. Earth and Planetary Science Letters 461, 30-39.

Chantel, J., Manthilake, G.M., Frost, D.J., Beyer, C., Ballaran, T.B., Jing, Z.C., Wang, Y.B., 2016. Elastic wave velocities in polycrystalline $Mg_3Al_2Si_3O_{12}$-pyrope garnet to 24 GPa and 1300 K. American Mineralogist 101, 991-997.

Canil, D., and H. S. C. ONeill, 1996: Distribution of ferric iron in some upper-mantle assemblages. Journal of Petrology 37, 609-635.

Du, W., S. M. Clark, and D. Walker, 2015: Thermo-compression of pyrope-grossular garnet solid solutions: Non-linear compositional dependence. American Mineralogist 100, 215-222.

Frost, D.J., 2008. The upper mantle and transition zone. Elements 4, 171-176.

Erba, A., Mahmoud, A., Orlando, R., Dovesi, R., 2014. Elastic properties of six silicate garnet end members from accurate ab initio simulations. Physics and Chemistry of Minerals 41, 151-160.

Greaux, S., T. Irifune, Y. Higo, Y. Tange, T. Arimoto, Z. D. Liu, and A. Yamada. Sound velocity of $CaSiO_3$ perovskite suggests the presence of basaltic crust in the Earth's lower mantle. Nature 565 (7738), 218-21.

Hirschmann, M.M., Stolper, E.M., 1996. A possible role for garnet pyroxenite in the origin of the "garnet signature" in MORB. Contributions to Mineralogy and Petrology 124, 185-208.

Ickert, R.B., Stachel, T., Stern, R.A., Harris, J.W., 2015. Extreme 18O-enrichment in majorite constrains a crustal origin of transition zone diamonds. Geochemical Perspectives Letters 1, 65-74.

Irifune, T., Sekine, T., Ringwood, A.E., Hibberson, W.O., 1986. The eclogite-garnetite transformation at high-pressure and some geophysical implications. Earth and Planetary Science Letters 77, 245-256.

Irifune, T., 1987. An experimental investigation of the pyroxene garnet transformation in a pyrolite composition and its bearing on the constitution of the mantle. Physics of The Earth and Planetary Interiors 45, 324-336.

Irifune, T., Higo, Y., Inoue, T., Kono, Y., Ohfuji, H., Funakoshi, K., 2008. Sound velocities of majorite garnet and the composition of the mantle transition region. Nature 451, 814-817.

Jiang, F.M., Speziale, S., Shieh, S.R., Duffy, T.S., 2004. Single-crystal elasticity of andradite garnet to 11 GPa. Journal of Physics-Condensed Matter 16, S1041-S1052.

Kavner, A., Sinogeikin, S.V., Jeanloz, R., Bass, J.D., 2000. Equation of state and strength of natural majorite. Journal of Geophysical Research-Solid Earth 105, 5963-5971.

Kiseeva, E.S., Vasiukov, D.M., Wood, B.J., McCammon, C., Stachel, T., Bykov, M., Bykova, E., Chumakov, A., Cerantola, V., Harris, J.W., Dubrovinsky, L., 2018. Oxidized iron in garnets from the mantle transition zone. Nature Geoscience 11, 144-150.

Kiseeva, E.S., Wood, B.J., Ghosh, S., Stachel, T., 2016. The pyroxenite-diamond connection. Geochemical Perspectives Letters 2, 1-9.

Kiseeva, E.S., Yaxley, G.M., Stepanov, A.S., Tkalcic, H., Litasov, K.D., Kamenetsky, V.S., 2013. Metapyroxenite in the mantle transition zone revealed from majorite inclusions in diamonds. Geology 41, 883-886.

Kono, Y., Greaux, S., Higo, Y., Ohfuji, H., Irifune, T., 2010. Pressure and temperature dependences of elastic properties of grossular garnet up to 17 GPa and 1650 K. J Earth Sci-China 21, 782-791.

Kurnosov, A., Marquardt, H., Frost, D.J., Ballaran, T.B., Ziberna, L., 2017. Evidence for a Fe^{3+}-rich pyrolitic lower mantle from (Al,Fe)-bearing bridgmanite elasticity data. Nature 543, 543-548.

Lindsay, S. M., M. W. Anderson and J. R. Sandercock (1981) Construction and alignment of a high performance multipass vernier tandem Fabry-Perot interferometer. Review of Scientific Instruments 52(10), 1478-1486.

Liu, Z. D., S. Greaux, N. Cai, N. Siersch, T. B. Ballaran, T. Irifune, and D. J. Frost (2019) Influence of aluminum on the elasticity of majorite-pyrope garnets. American Mineralogist 104, 929-935.

Murakami, M., Sinogeikin, S.V., Litasov, K., Ohtani, E., Bass, J.D., 2008. Single-crystal elasticity of iron-bearing majorite to 26 GPa: Implications for seismic velocity structure of the mantle transition zone. Earth and Planetary Science Letters 274, 339-345.

Pamato, M.G., Kurnosov, A., Ballaran, T.B., Frost, D.J., Ziberna, L., Giannini, M., Speziale, S., Tkachev, S.N., Zhuravlev, K.K., Prakapenka, V.B., 2016. Single crystal elasticity of majoritic garnets: Stagnant slabs and thermal anomalies at the base of the transition zone. Earth and Planetary Science Letters 451, 114-124.

Pearson, D.G., Davies, G.R., Nixon, P.H., 1993. Geochemical constraints on the petrogenesis of diamond facies pyroxenites from the Beni Bousera peridotite massif, North Morocco. Journal of Petrology 34, 125-172.

Ringwood, A.E., 1991. Phase transformations and their bearing on the constitution and dynamics of the mantle. Geochimica Et Cosmochimica Acta 55, 2083-2110.

Rohrbach, A., Ballhaus, C., Golla-Schindler, U., Ulmer, P., Kamenetsky, V.S., Kuzmin, D.V., 2007. Metal saturation in the upper mantle. Nature 449, 456-458.

Rohrbach, A., Schmidt, M.W., 2011. Redox freezing and melting in the Earth's deep mantle resulting from carbon-iron redox coupling. Nature 472, 209-212.Sinogeikin, S.V., Bass, J.D., 2000. Single-crystal elasticity of pyrope and MgO to 20 GPa by Brillouin scattering in the diamond cell. Physics of the Earth and Planetary Interiors 120, 43-62.

Sanchez-Valle, C., J. Y. Wang, and A. Rohrbach, 2019: Effect of calcium on the elasticity of majoritic garnets and the seismic gradients in the mantle transition zone. Physics of the Earth and Planetary Interiors 293, 1-5.

Sinogeikin, S.V., Bass, J.D., 2002. Elasticity of pyrope and majorite–pyrope solid solutions to high temperatures. Earth and Planetary Science Letters 203, 549-555.

Speziale, S., Marquardt, H., Duffy, T.S., 2014. Brillouin scattering and its application in geosciences. Spectroscopic Methods in Mineralology and Materials Sciences 78, 543-603.

Sobolev, N. V., Y. G. Lavrent'ev, N. P. Pokhilenko, and L. V. Usova, 1973: Chrome-rich garnets from kimberlites of Yakutia and their parageneses. Contributions to Mineralogy and Petrology, 40, 39-52.

Stixrude, L., Lithgow-Bertelloni, C., 2005. Thermodynamics of mantle minerals - I. Physical properties. Geophysical Journal International 162, 610-632.

Tappert, R., Stachel, T., Harris, J.W., Muehlenbachs, K., Ludwig, T., Brey, G.P., 2005. Subducting oceanic crust: The source of deep diamonds. Geology 33, 565-568.

Thomson, A.R., Walter, M.J., Kohn, S.C., Brooker, R.A., 2016. Slab melting as a barrier to deep carbon subduction. Nature 529, 76-79.

Vasiukov, D.M., Ismailova, L., Kupenko, I., Cerantola, V., Sinmyo, R., Glazyrin, K., McCammon, C., Chumakov, A.I., Dubrovinsky, L., Dubrovinskaia, N., 2018. Sound velocities of skiagite–iron–majorite solid solution to 56 GPa probed by nuclear inelastic scattering. Physics and Chemistry of Minerals 45, 397-404.

Wang, Z.C., Ji, S.C., 2001. Elasticity of six polycrystalline silicate garnets at pressure up to 3.0 GPa. American Mineralogist 86, 1209-1218.

Whitfield, C. H., E. M. Brody and W. A. Bassett (1976) Elastic moduli of NaCl by Brillouin scattering at high pressure in a diamond anvil cell. Review of Scientific Instruments 47(8), 942-947.

Wit, R. W. L., Trampert, J., & Hilst, R. D. 2012. Toward quantifying uncertainty in travel time tomography using the null-space shuttle. Journal of Geophysical Research: Solid Earth, 117 (B3).

Wood, B.J., Kiseeva, E.S., Matzen, A.K., 2013. Garnet in the Earth's Mantle. Elements 9, 421-426.

Woodland, A.B. and H.S.C. Oneill (1993). Synthesis and Stability of $Fe_3^{2+}Fe_2^{3+}Si_3O_{12}$ garnet and phase relations with $Fe_3Al_2Si_3O_{12}$-$Fe_3^{2+}Fe_2^{3+}Si_3O_{12}$ solutions. American Mineralogist, 78(9-10), 1002-1015.

Yaxley, G.M., Green, D.H., 1998. Reactions between eclogite and peridotite: mantle refertilisation by subduction of oceanic crust. Schweizerische Mineralogische Und Petrographische Mitteilungen 78, 243-255.

Figure captions

Figure 1. Sketch across 100-500 km depth with phase proportions in basaltic (eclogitic) and pyrolytic bulk compositions. With increasing depth, pyroxene increasingly dissolves in the garnet structure. This transition is strongly composition-dependent, and the complete disappearance of clinopyroxene from the system was reported at pressures between 13 and 26 GPa. Upon clinopyroxene-out, the rocks convert to wadsleyite-majorite garnet in peridotitic

assemblages or near-monomineralic garnetite (with small amounts of stishovite) in eclogitic or olivine-free pyroxenitic assemblages. Stability fields from Stixrude and Lithgow-Bertelloni (2005) and Ringwood (1991).

Figure 2. (a) Optical microscope image of inclusion JF-55A, (b) Typical Brillouin spectrum of sample JF 55a.

Figure 3. Sound velocity as a function of the pressure of last equillibration estimated from garnet compositions (Beyer and Frost, 2017). The relative percentage of ferric iron ($100*Fe^{3+}/Fe_{tot}$) for the studied majoritic garnets is 12% for 37b, 20% for 39b and 30% for 55a. Error bars for sound velocities are standard errors (Table 2).

Figure 4. Illustration of the seismic velocity and impedance contrasts expected in a scenario where a pyroxenitic majorite layer forms through the reaction of peridotite/pyrolite with eclogite/metabasalt. (a) Cartoon to illustrate the formation of a pyroxenitic majorite layer at the interface between eclogite and peridotite. The modelled seismic impedance contrasts at the boundaries between peridotite and pyroxenite (red) and pyroxenite and eclogite (orange) are given in the figure. Modelling has been done for typical mantle assemblages expected at 350 km (median depth of origin of our majorite inclusions), but using elastic properties and densities at ambient conditions. (b) Compressional and shear wave velocities of the three natural majoritic garnets measured in this study (black solid diamonds) in comparison to the expected seismic velocities for peridotite/pyrolite (green diamonds) and eclogite/metabasalt (blue diamonds). “Depth of formation” in (b) refers to the depths at which the here-studied garnets likely formed in Earth’s mantle. The seismic wave velocities of peridotite/pyrolite and eclogite/metabasalt were calculated using ambient conditions elastic properties, but employing a mineralogy expected at the respective depths. See text for more details.

DOI: https://doi.org/10.2138/am-2020-7136CCBY

Table captions

Table 1. Normalised molar fractions of studied majoritic inclusions in diamonds. For chemical composition in wt% oxides, see Supplementary Table 1. For simplicity, Na-majorite was omitted from sound velocity calculations with the sums normalised to 100%. Based on EPMA data, uncertainties on the values are no higher than 5%.

Table 2. Measured acoustic wave velocities as function of rotation angle. The uncertainty of individual measurements at specific chi angles was estimated from signal-to-noise ratio following Kurnosov et al. (2017) and is lower than 1% (values in brackets). Due to unperfect sample polishement, data is scattered and therefore aggregate velocity is estimated as an average with standard error (see text for discussion, Supplementary figure 1).

Table 3. Literature data for elastic parameters of individual garnet end-members (Arimoto et al., 2015; Chantel et al., 2016; Jiang et al., 2004; Kono et al., 2010; Liu et al., 2019). Numbers in brackets indicate standard deviation used in this study.

Table 4. Physical parameters and acoustic velocities of pyroxenitic, peridotitic and eclogitic mantle rocks calculated at ambient conditions, but employing the mineralogy expected at the pressure of formation P_{form} of the here-measured garnets, see Supplementary Table 3.

DOI: https://doi.org/10.2138/am-2020-7136CCBY

Figure 1

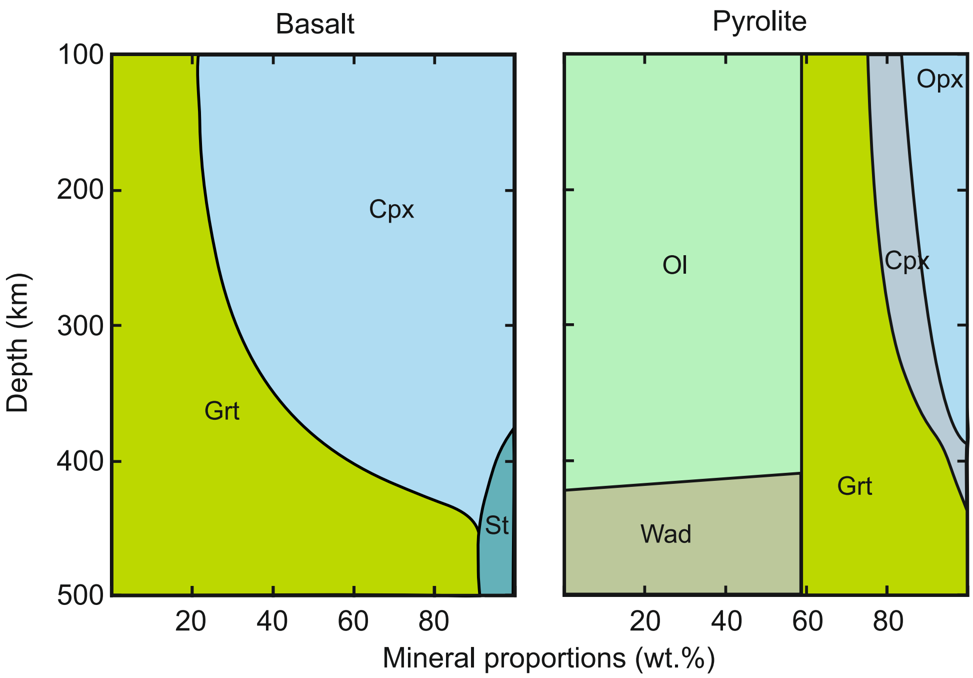

DOI: https://doi.org/10.2138/am-2020-7136CCBY

Figure 2

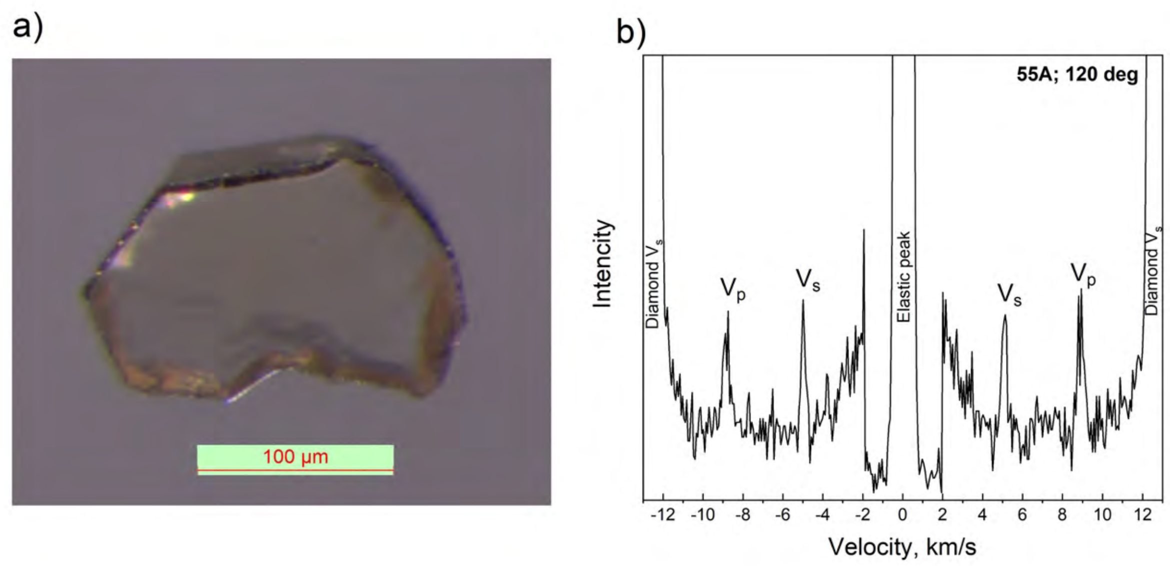

This is a preprint, the final version is subject to change, of the American Mineralogist (MSA)
Cite as Authors (Year) Title. American Mineralogist, in press.
DOI: https://doi.org/10.2138/am-2020-7136CCBY

Figure 3

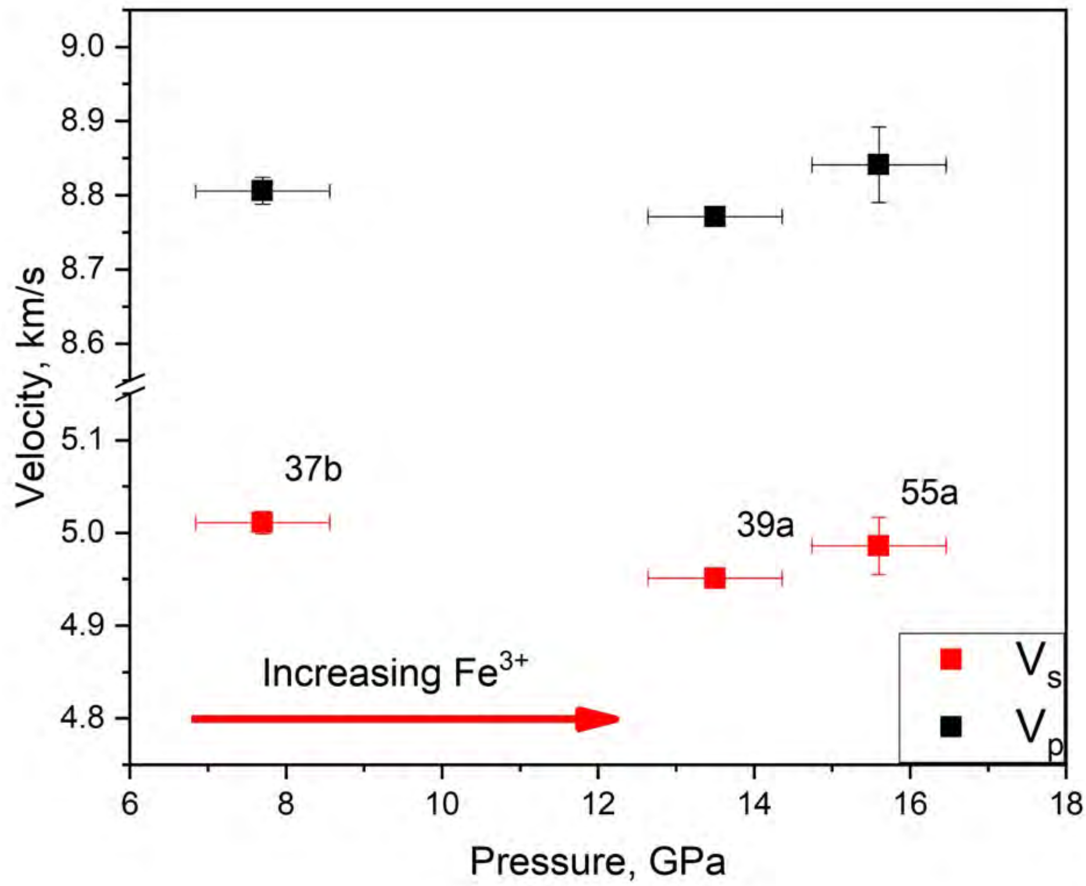

Figure 4

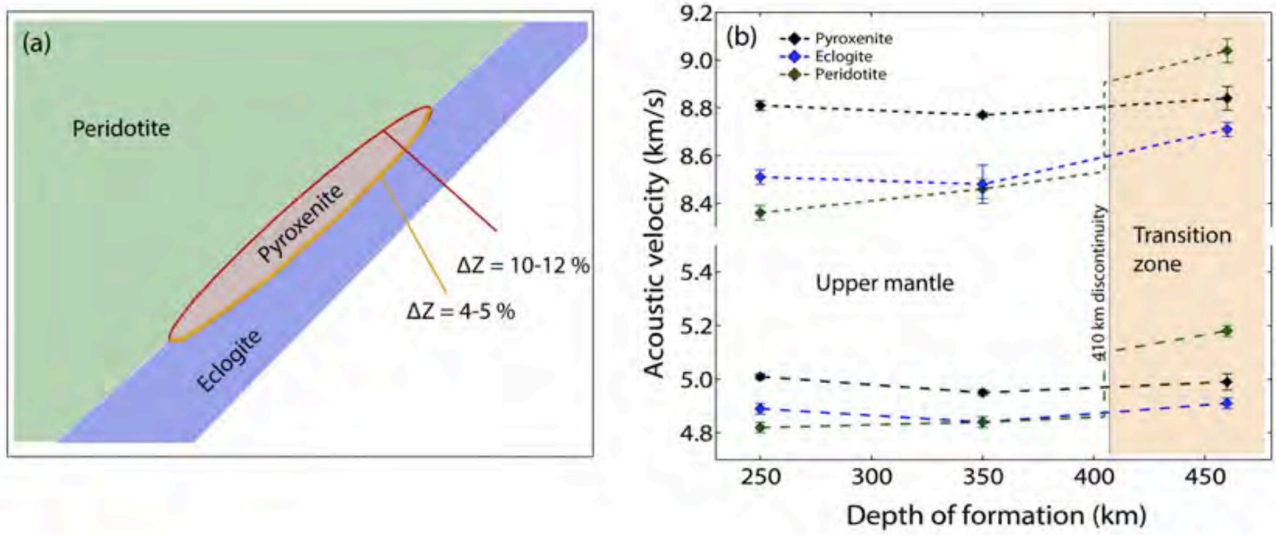
(a)
Peridotite
Pyroxenite
Eclogite
ΔZ = 10-12 %
ΔZ = 4-5 %
(b)
Pyroxenite
Eclogite
Peridotite
Acoustic velocity (km/s)
9.2
9.0
8.8
8.6
8.4
5.4
5.2
5.0
4.8
Upper mantle
410 km discontinuity
Transition zone
250
300
350
400
450
Depth of formation (km)

DOI: https://doi.org/10.2138/am-2020-7136CCBY

Table 1. Normalised molar fractions of studied majoritic inclusions in diamonds. For chemical composition in wt% oxides, see Supplementary Table 1. For simplicity, Na-majorite was omitted from sound velocity calculations with the sums normalised to 100%. Based on EPMA data, uncertainties on the values are no higher than 5%.

	Pyrope $Mg_3Al_2(SiO_4)_3$	**Andradite** $Ca_3Fe_2(SiO_4)_3$	**Na-majorite** $Na_2MgSi_5O_{12}$	**Almandine** $Fe_3Al_2(SiO_4)_3$	**Mg-Majorite** $Mg_3(MgSi)(SiO_4)_3$	**Grossular** $Ca_3Al_2(SiO_4)_3$
JF 37b	0.524	0.047	0.010	0.0230	0.062	0.120
JF 39a	0.379	0.066	0.026	0.177	0.264	0.082
JF 55a	0.265	0.084	0.030	0.130	0.381	0.104

Table 2. Measured acoustic wave velocities as function of rotation angle. The uncertainty of individual measurements at specific chi angles was estimated from signal-to-noise ratio following Kurnosov et al. (2017) and is lower than 1% (values in brackets). Due to unperfect sample polishement, data is scattered and therefore aggregate velocity is estimated as an average with standard error (see text for discussion, Supplementary figure 1).

37b		
Angle (deg)	Vs (km/s)	Vp (km/s)
0	5.144(38)	8.776(14)
20	5.079(10)	8.653(11)
40	5.017(5)	8.863(8)
60	5.045(32)	8.898(33)
70	5.044(6)	8.928(8)
80	4.999(3)	8.895(8)
100	5.000(6)	8.846(14)
120	5.066(10)	8.921(14)
140	5.017(5)	8.827(8)
180	4.979(6)	8.836(14)
-10	5.007(8)	8.743(14)
-30	5.044(4)	8.687(4)
-50	5.017(3)	8.813(3)
-70	4.972(5)	8.808(11)
-90	4.941(33)	8.813(33)
-110	4.947(14)	8.781(21)
-130	4.968(5)	8.746(8)
-150	4.958(3)	8.750(5)
-170	4.960(61)	8.731(61)
Average	5.011	8.806
STDEV/$n^{1/2}$	0.012	0.018

39a		
Angle (deg)	Vs (km/s)	Vp (km/s)
0	4.962(8)	8.771(7)
20	4.967(6)	8.746(7)
40	4.944(4)	8.751(8)
60	4.951(12)	8.779(19)
80	4.921(21)	8.781(8)
100	4.929(7)	8.692(14)
120	4.930(9)	8.711(15)
140	4.905(2)	8.755(6)
160	4.881(2)	8.711(8)
-10	4.979(2)	8.816(10)
-30	4.987(2)	8.869(2)
-50	5.010(8)	8.860(22)
-70	5.011(6)	8.816(2)
-90	4.987(2)	8.830(11)
-110	4.957(2)	8.802(5)
-130	4.949(2)	8.799(3)
-150	4.932(3)	8.725(4)
-170	4.935(2)	8.715(3)
-180	4.928(2)	8.711(10)
Average	4.951	8.771
STDEV/$n^{1/2}$	0.008	0.012

55a		
Angle (deg)	Vs (km/s)	Vp (km/s)
0	4.985(3)	8.849(9)
20	5.127(3)	8.985(8)
40	5.166(3)	9.108(8)
80	5.095(3)	9.069(11)
120	5.07(21)	8.953(33)
140	5.046(21)	8.926(33)
160	4.926(4)	8.825(11)
180	4.908(11)	8.742(21)
-10	5.010(4)	8.937(14)
-30	4.940(3)	8.809(8)
-50	4.896(3)	8.626(8)
-70	4.843(14)	8.596(17)
-90	4.811(14)	8.502(21)
Average	4.986	8.841
STDEV/$n^{1/2}$	0.031	0.051

DOI: https://doi.org/10.2138/am-2020-7136CCBY

Table 3. Literature data for elastic parameters of individual garnet end-members (Arimoto et al., 2015; Chantel et al., 2016; Jiang et al., 2004; Kono et al., 2010; Liu et al., 2019). Numbers in brackets indicate standard deviation used in this study.

	Chantel, 2016 Pyrope $Mg_3Al_2(SiO_4)_3$	**Jiang 2004 Andradite $Ca_3Fe_2(SiO_4)_3$**	**Arimoto 2015 Almandite $Fe_3Al_2(SiO_4)_3$**	**Liu et al., 2019 Majorite $Mg_3(MgSi)(SiO_4)_3$**	**Kono, 2010 Grossular $Ca_3Al_2(SiO_4)_3$**
K_0 (GPa)	172(1.6)	154.5(6)	172.6(1.1)	158(2)	171.5(8)
G_0 (GPa)	89.1(5)	89.7(4)	94.2(3)	83(1)	108.4(3)
ρ (g cm^{-3})	3.565(5)	3.843(5)	4.3188(2)	3.518(6)	4.008(5)

Table 4. Physical parameters and acoustic velocities of pyroxenitic, peridotitic and eclogitic mantle rocks calculated at ambient conditions, but employing the mineralogy expected at the pressure of formation P_{form} of the here-measured garnets, see Supplementary Table 3.

P_{form} = 8 GPa	**ρ (g/cm^3)**	**K_{VRH} (GPa)**	**G_{VRH} (GPa)**	***Vp* (km/s)**	***Vs* (km/s)**
Pyroxenite	3.774(5)	167(1)	94.6(5)	8.81(2)	5.01(1)
Peridotite	3.432(2)	133(2)	79.8(7)	8.36(3)	4.82(2)
Eclogite	3.505(2)	142(1.4)	84(1)	8.51(3)	4.89(2)
P_{form} = 13 GPa	**ρ (g/cm^3)**	**K_{VRH} (GPa)**	**G_{VRH} (GPa)**	***Vp* (km/s)**	***Vs* (km/s)**
Pyroxenite	3.738(5)	165(1)	91.5(5)	8.77(1)	4.95(1)
Peridotite	3.471(2)	140(2)	81(1)	8.46(4)	4.84(2)
Eclogite	3.689(3)	150(4)	86(2)	8.48(8)	4.84(6)
P_{form} = 16 GPa	**ρ (g/cm^3)**	**K_{VRH} (GPa)**	**G_{VRH} (GPa)**	***Vp* (km/s)**	***Vs* (km/s)**
Pyroxenite	3.701(5)	167(3)	92.2(1)	8.84(5)	4.99(3)
Peridotite	3.633(8)	167(2)	97(1)	9.04(5)	5.18(3)
Eclogite	3.809(3)	166(3)	92(1)	8.71(3)	4.91(2)